



TIME WAITS FOR NO ONE

Enlist the experts at Bio X Cell for  
Antibody Production Services

EXPLORE

RECEIVE 10% OFF NOW with code: CONTRACT22JI



## Profiles of Long Noncoding RNAs in Human Naive and Memory T Cells

Charles F. Spurlock III, Guzel Shaginurova, John T. Tossberg, Jonathan D. Hester, Nathaniel Chapman, Yan Guo, Philip S. Crooke III and Thomas M. Aune

This information is current as of February 26, 2022.

*J Immunol* 2017; 199:547-558; Prepublished online 9 June 2017;

doi: 10.4049/jimmunol.1700232

<http://www.jimmunol.org/content/199/2/547>

**Supplementary Material** <http://www.jimmunol.org/content/suppl/2017/06/09/jimmunol.1700232.DCSupplemental>

**References** This article **cites 56 articles**, 9 of which you can access for free at:  
<http://www.jimmunol.org/content/199/2/547.full#ref-list-1>

**Why *The JI*? Submit online.**

- **Rapid Reviews! 30 days\*** from submission to initial decision
- **No Triage!** Every submission reviewed by practicing scientists
- **Fast Publication!** 4 weeks from acceptance to publication

*\*average*

**Subscription** Information about subscribing to *The Journal of Immunology* is online at:  
<http://jimmunol.org/subscription>

**Permissions** Submit copyright permission requests at:  
<http://www.aai.org/About/Publications/JI/copyright.html>

**Email Alerts** Receive free email-alerts when new articles cite this article. Sign up at:  
<http://jimmunol.org/alerts>



# Profiles of Long Noncoding RNAs in Human Naive and Memory T Cells

Charles F. Spurlock, III,\* Guzel Shaginurova,\* John T. Tossberg,\* Jonathan D. Hester,\* Nathaniel Chapman,\* Yan Guo,<sup>†</sup> Philip S. Crooke, III,<sup>‡</sup> and Thomas M. Aune\*,<sup>§</sup>

We employed whole-genome RNA-sequencing to profile mRNAs and both annotated and novel long noncoding RNAs (lncRNAs) in human naive, central memory, and effector memory CD4<sup>+</sup> T cells. Loci transcribing both lineage-specific annotated and novel lncRNA are adjacent to lineage-specific protein-coding genes in the genome. Lineage-specific novel lncRNA loci are transcribed from lineage-specific typical- and supertranscriptional enhancers and are not multiexonic, thus are more similar to enhancer RNAs. Novel enhancer-associated lncRNAs transcribed from the *IFNG* locus bind the transcription factor NF- $\kappa$ B and enhance binding of NF- $\kappa$ B to the *IFNG* genomic locus. Depletion of the annotated lncRNA, *IFNG*-AS1, or one *IFNG* enhancer-associated lncRNA abrogates *IFNG* expression by memory T cells, indicating these lncRNAs have biologic function. *The Journal of Immunology*, 2017, 199: 547–558.

Immunologic memory is a critical feature of the adaptive immune response conferring long-lasting protective immunity to the host. Memory T (T<sub>M</sub>) cells (CD4<sup>+</sup> or CD8<sup>+</sup>) can be broadly divided into central memory T (T<sub>CM</sub>) and effector memory T (T<sub>EM</sub>) cells (1, 2). T<sub>CM</sub> cells are CD45RO<sup>+</sup>, constitutively express CCR7 and CD62L, recirculate through lymphoid organs, express high levels of IL-2 after restimulation, proliferate vigorously compared with T<sub>EM</sub> cells, express low levels of IFN- $\gamma$ , and have limited effector function (3–5). T<sub>EM</sub> cells are also CD45RO<sup>+</sup>, but express low levels of CCR7 and expression of CD62L is heterogeneous. T<sub>EM</sub> cells preferentially reside in nonlymphoid

tissues and rapidly produce effector cytokines in response to Ag stimulation (6). Despite our clear understanding of the critical importance of T<sub>M</sub> cells to the adaptive immune system, our understanding of mechanisms driving differentiation into T<sub>EM</sub> and T<sub>CM</sub> lineages and maintaining these phenotypes is incomplete (3, 7).

The vast majority of the genomic sequence is transcribed into either protein-coding RNAs or noncoding RNAs (ncRNAs) (8). Long ncRNAs (>200 bp to distinguish them from short RNAs such as micro-RNAs or tRNAs) can be subdivided into long noncoding RNAs (lncRNAs), enhancer RNAs (eRNAs) and other species. Certain lncRNAs exhibit many features of mRNAs and are 5' capped, spliced, and polyadenylated but exhibit little if any coding potential (9–12). About 20,000 lncRNA genes have been identified in vertebrate genomes, similar to the number of protein-coding genes. A growing array of regulatory functions has been ascribed to this new class of RNAs (9, 10, 13). The eRNAs, so-called because they are transcribed near transcriptional enhancer elements and lack promoters in the classic sense, are divided into two classes: 1d-eRNAs and 2d-eRNAs (14–17). The 2d-eRNAs are transcribed in both sense and antisense orientations, tend to be relatively short (500–2000 bp), are relatively unstable, and are not polyadenylated. The 1d-eRNAs are transcribed in one direction only, are polyadenylated, and are relatively stable. Thus, if strand-specific information is available, it is relatively straightforward to distinguish 2d-eRNAs from 1d-eRNAs. At this point, a clear set of rules has not emerged to distinguish lncRNAs from 1d-eRNAs, although types of epigenetic modifications and cellular locations may aid classification. In contrast to lncRNAs, biologic functions of 1d- and 2d-eRNAs are less well understood and it has been argued that enhancer transcription may simply represent transcriptional noise without true biologic function ascribed to the transcribed RNA (18, 19).

DNA enhancer elements are defined by their ability to direct cell type-specific gene expression programs determining cell identity. Stretch-enhancers, also referred to as superenhancers (SE), are a subset of enhancers exhibiting proximity to certain protein-coding genes that drive cell identity (20, 21). SEs differ from typical enhancers (TE) in size, transcription factor density, and ability to activate transcription. Both are marked by histone acetyltransferases, p300 and CBP, and H3K27-acetylation (H3K27Ac) (22, 23). Bromodomain-containing proteins (BRD), such as BRD2, BRD3, BRD4 and BRDT, are recruited to TE and SE H3K27Ac marks to

\*Department of Medicine, Vanderbilt University School of Medicine, Nashville, TN 37232; <sup>†</sup>Department of Cancer Biology, Vanderbilt University School of Medicine, Nashville, TN 37232; <sup>‡</sup>Department of Mathematics, Vanderbilt University, Nashville, TN 37240; and <sup>§</sup>Department of Pathology, Microbiology and Immunology, Vanderbilt University School of Medicine, Nashville, TN 37232

ORCID: 0000-0001-9015-6321 (C.F.S.); 0000-0001-8314-1308 (G.S.); 0000-0002-6151-9135 (J.D.H.); 0000-0002-4968-4306 (T.M.A.).

Received for publication February 21, 2017. Accepted for publication May 12, 2017.

This work was supported by grants from the National Institutes of Health (R01 AI044924, DK007383, and DK20593), the National Science Foundation (DGE0909667), and by Clinical and Translational Science Award UL1TR000445. Vanderbilt Technologies for Advanced Genomics' core facility was supported in part by grants from the National Institutes of Health (P30 CA68485, P30 EY08126 and G20 RR030956).

C.F.S. and T.M.A. designed the research; C.F.S., G.S., J.T.T., N.C., and J.D.H. performed the research; C.F.S., G.S., J.D.H., Y.G., P.S.C., and T.M.A. analyzed the data; C.F.S. and T.M.A. wrote the paper; all authors reviewed, edited and approved the final version of the paper.

The RNA sequencing data presented in this article have been submitted to the National Center for Biotechnology Information's Gene Expression Omnibus (<https://www.ncbi.nlm.nih.gov/geo>) under accession number GSE85294.

Address correspondence and reprint requests to Prof. Thomas M. Aune, Medical Center North T3113, Vanderbilt University Medical Center, Vanderbilt University School of Medicine, 1161 21st Avenue South, Nashville, TN 37232. E-mail address: tom.aune@vanderbilt.edu

The online version of this article contains supplemental material.

Abbreviations used in this article: BRD, bromodomain-containing protein; ChIP, chromatin immunoprecipitation; eRNA, enhancer RNA; FDR, false discovery rate; FPKM, fragments per kilobase per million reads; H3K27Ac, H3K27-acetylation; lncRNA, long noncoding RNA; MSigDB, Molecular Signature Database; ncRNA, noncoding RNA; RNA-seq, RNA sequencing; SE, superenhancer; siRNA, small interfering RNA; T<sub>CM</sub>, central memory T; TE, typical enhancer; T<sub>EM</sub>, effector memory T; T<sub>M</sub>, memory T; T<sub>N</sub>, naive T.

Copyright © 2017 by The American Association of Immunologists, Inc. 0022-1767/17/\$30.00

facilitate recruitment of RNA pol2 and activate transcription (24). Genes with SE structures are also enriched near single nucleotide polymorphisms linked to autoimmune disorders, including rheumatoid arthritis, and expression of risk genes is modulated by the JAK inhibitor tofacitinib, which is used to manage rheumatoid arthritis (22).

In our present study, we sought to identify mRNAs, and annotated and novel lncRNAs preferentially expressed in naive T ( $T_N$ ),  $T_{CM}$ , and  $T_{EM}$  cells. Our results support the idea that lineage-specific mRNAs, known lncRNAs, and novel lncRNAs are coexpressed, and these loci are colocalized in the genome with SEs and TEs. Further, inhibition of SE or TE function abrogates expression of annotated and novel lncRNAs and mRNAs at key gene loci required for lineage-specific cell phenotypes. One mechanism by which these novel lncRNAs act is to bind the transcription factor, NF- $\kappa$ B, and reinforce binding of NF- $\kappa$ B to chromatin. We also show that depletion of either the annotated lncRNA, IFNG-AS1, or one of the IFNG-associated novel lncRNAs abrogates IFNG transcription by  $T_M$  cells, a critical function of the adaptive immune response.

## Materials and Methods

### Cell isolation and culture

Human PBMC were isolated from healthy control subjects with no chronic or acute conditions using Ficoll-Hypaque centrifugation. All subjects included in the study, both in initial RNA-sequencing (RNA-seq) and follow-up analyses, were male, of Caucasian descent, and between ages of 25–32.  $T_N$ ,  $T_{CM}$ , and  $T_{EM}$  cells used for RNA-seq studies were isolated using the BD Pharmingen Human Naive/Memory T cell panel (561438; BD) according to the manufacturer's supplied protocol, followed by FACS. The relative purity of cell populations was assessed prior to RNA-seq. For certain studies as described in the text,  $T_N$  cells and total  $T_M$  ( $T_{CM}$  +  $T_{EM}$ ) cells were also isolated from total PBMC using the EasySep Naive CD4<sup>+</sup> T cell isolation kit (19555; StemCell Technologies) or the EasySep Memory CD4<sup>+</sup> T cell enrichment kit (19157; StemCell Technologies) using the provided protocol. Tissue culture experiments were conducted in RPMI 1640 medium supplemented with 10% FBS, penicillin streptomycin, and L-glutamine. I-BET was obtained from EMD Chemicals (cat no. 401010; Calbiochem) and ( $\pm$ )-JQ1 (SML0974) was obtained from Sigma-Aldrich. The study was approved by the institutional review board at Vanderbilt University Medical Center. Written informed consent was obtained at the time of blood sample collection.

### Chromatin immunoprecipitation

Chromatin immunoprecipitation (ChIP) procedures were followed as described using anti-H3K27-Ac Ab (ab6002; Abcam), anti-RNA polymerase II (ab24759; Abcam), anti-NF- $\kappa$ B, p65 subunit (ab47423), anti-Tbet (ab91103; Abcam), or anti-mouse IgG (10  $\mu$ g; sc-2025; Santa Cruz Biotechnology) (25, 26). Quantitative real-time PCR with SYBR Green was used to measure DNA after ChIP and DNA purification. Primers used to amplify DNA are listed in Supplemental Tables I and II. Quantitative ChIP assays were performed in triplicate and results from three or more independent experiments were averaged. We also performed a modified ChIP assay. Cells were solubilized in nonionic detergents to isolate chromatin. Chromatin was treated with RNase for 10 min, fixed with formaldehyde, sonicated, and processed for ChIP assay using the same procedures described above.

### RNA isolation and quantitative RT-PCR

Total RNA was isolated with TRI Reagent (MRC) and purified with the RNeasy MinElute Cleanup kit (Qiagen) using an on-column DNase treatment to ensure the absence of genomic DNA contamination. cDNA was synthesized from total RNA using the SuperScript III First-Strand Synthesis Kit (Life Technologies) using oligo-dT primers, and purified using the Qiagen QiaQuick PCR purification kit. Transcript levels were measured in duplicate by quantitative RT-PCR using TaqMan assays (ABI 7300 Real Time PCR System; Life Technologies) or using SYBR Green (PowerUp SYBY Green; ABI 7300; Life Technologies). Expression levels were calculated relative to GAPDH using the  $\Delta\Delta$  cycle threshold method. Primer pairs used in SYBR Green reactions are listed in Supplemental Table II.

### Immunoprecipitations

Immunoprecipitations were performed as previously described (26, 27).

### Cell transfections

Flow cytometry experiments involving FACS and/or intracellular cytokine measurements small interfering RNA (siRNA) transfection were performed as described previously (26).

### RNA-seq sample preparation and data analysis

RNA was isolated using Tri-Reagent. Library preparation was performed using the Illumina Tru-Seq Stranded Total RNA kit. Whole genome RNA sequencing was performed by the Vanderbilt Technologies for Advanced Genomics. An Illumina HiSeq2500 instrument was used to generate 100 bp paired-end reads. A quality control step was performed at all stages of sequencing analysis including raw data, alignment, and expression quantification using tools such as QC3 and MultiRankSEquation (28–30). The RNA data were aligned with TopHat 2 and gene expression levels were quantified using Cufflinks (31–33). Differentially expressed genes measured using Cufflinks/Cuffdiff were expressed as fragments per kilobase per million reads (FPKM) and a cutoff of 0.5 FPKM and 1.0 FPKM was employed for lncRNA and mRNA measurements, respectively. Gene definition lists and results using the GRCh37/hg19 and GRCh38/hg38 were compared and generated similar results. Results from the GRCh37/hg19 builds are presented to permit a more direct comparison with previously described TE and SE locations (21), which were also derived from the GRCh37/hg19 build. False discovery rate (FDR < 0.05) was used to correct for multiple testing. De novo transcriptome assembly was performed on whole genome RNA-seq data from Illumina Tru-Seq Stranded Total RNA libraries with TopHat 2 and Cufflinks using upper quartile normalization (34) and fragment bias correction (35). Novel transcripts were assembled from reads prealigned to human genome 19 (GRCh37/hg19) using TopHat. Identification of novel lncRNA transcripts was accomplished using established methodologies (8, 36). Summarized pipelines for discovery of novel lncRNAs and prediction of transcripts with protein-coding potential were reported previously (26).

For example, to identify  $T_N$ -specific lncRNAs, we calculated lineage-specific lncRNAs using the equation (FPKM in  $T_N$ )/[FPKM in ( $T_{CM}$  +  $T_{EM}$ )/2] and so on for  $T_{CM}$ - and  $T_{EM}$ -specific memory lncRNAs. We required that each lncRNA exhibit a >5-fold difference between groups. Relative lncRNA expression levels are shown for a portion of these lncRNAs using a heatmap, with each column representing an individual lncRNA and each row representing expression levels of each of three replicate  $T_N$ ,  $T_{CM}$ , or  $T_{EM}$  cell samples (Fig. 1B). Expression of these lncRNAs clustered according to cell type with  $T_{EM}$  cells expressing the greatest number of cell type-specific lncRNAs followed by  $T_N$  cells and  $T_{CM}$  cells.

Genomic locations of total CD4<sup>+</sup>, naive CD4, and memory CD4 super enhancers and typical enhancers were previously reported (20).

### Statistical analysis

Unless otherwise indicated, data are expressed as the mean  $\pm$  SD of three or more independent experiments. Unless otherwise noted, significance was determined by Student *t* test using GraphPad Prism Software (La Jolla, CA). A *p* value <0.05 was considered significant.  $\chi^2$  analysis was performed using GraphPad Prism Software. Fisher exact test was performed with Excel; see <http://udel.edu/~mcdonald/statfishers.html>.

### Data availability

The RNA-seq data generated by this study are accessible through National Center for Biotechnology Information's Gene Expression Omnibus using the accession code GSE85294 (<https://www.ncbi.nlm.nih.gov/geo>).

## Results

### Lineage-specific annotated lncRNAs in naive and memory CD4 T cells

To initiate our studies, we isolated  $T_N$ ,  $T_{CM}$ , and  $T_{EM}$  cells from age- and gender-matched healthy donors. We performed whole-genome RNA-seq to identify lineage-specific RNAs. We found that ~12,000 of ~20,000 mRNAs, ~2,800 of ~20,000 annotated lncRNAs, and ~57,000 novel lncRNAs were expressed with means >1 FPKM in at least one T cell lineage (Fig. 1A, left panel). Average expression levels of annotated and novel lncRNAs were comparable and substantially lower than mRNAs (Fig. 1A, middle panel). About 70, 1, and 30% of total RNA detected were represented by mRNA, annotated lncRNA, and novel lncRNA

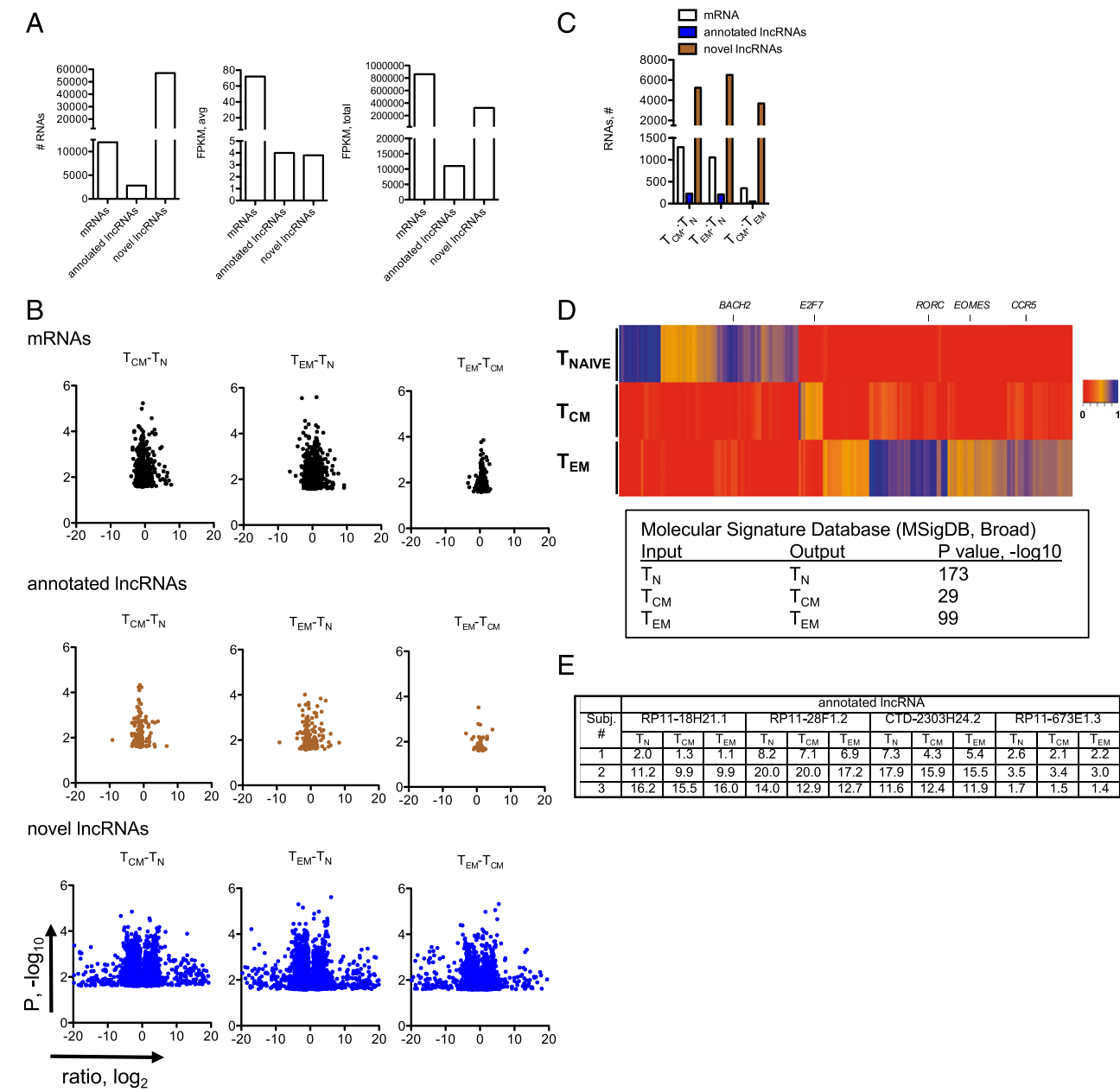


**FIGURE 1.** Cell type-specific expression of mRNAs and lncRNAs. **(A)** Left panel, total numbers of mRNAs (GRCh38 release, total protein-coding genes = 19,950), annotated lncRNAs (GRCh38 release, long noncoding genes = 15,767), and novel lncRNAs detected in this study by de novo assembly with average FPKM > 1 in at least one cell lineage; middle panel, average expression levels of the different RNA classes in  $T_N$ ,  $T_{CM}$ , and  $T_{EM}$  cells; right panel, total expression levels of the indicated RNA classes in  $T_N$ ,  $T_{CM}$ , and  $T_{EM}$  cells ( $n = 3$ ). **(B)** Volcano plots identifying lineage-specific RNA classes after FDR correction,  $p < 0.05$ . The x-axis represents the indicated expression ratios,  $\log_2$ , and the y-axis is the  $p$  value,  $-\log_{10}$ . **(C)** Total numbers of mRNAs, annotated lncRNAs, and novel lncRNAs that show lineage-specific expression [from (B)]. **(D)** Hierarchical clustering showing expression levels of mRNAs expressed by human CD4<sup>+</sup> T cells determined by whole genome RNA-seq aligned to hg38 ( $n = 3$ ). A scale bar is adjacent to the heat map. MSigDB analysis of lineage-specific mRNAs (identified in the heatmap) as input, outputs from the MSigDB analysis are shown with corresponding  $p$  values. **(E)** Individual variation in lncRNA expression. Expression levels in FPKM of four annotated lncRNAs are shown in  $T_N$ ,  $T_{CM}$ , and  $T_{EM}$  subsets isolated from three individual subjects.

classes, respectively (Fig. 1A, right panel). We also analyzed differences in expression of individual RNA classes in  $T_N$ ,  $T_{CM}$ , and  $T_{EM}$  lineages after FDR corrections. We found that lineage-specific quantitative differences in expression of novel lncRNAs were greater than lineage-specific differences in expression of either mRNAs or annotated lncRNAs (Fig. 1B). After FDR correction, we found that total numbers of lineage-specific novel lncRNAs were much greater than total numbers of lineage-specific mRNAs or annotated lncRNAs (Fig. 1C). As an initial quality assessment, we further analyzed lineage-specific expression of

mRNAs. The heatmap identifies mRNAs selectively expressed in  $T_N$ ,  $T_{CM}$ , and  $T_{EM}$  lineages (Fig. 1D). As expected (37–39), *BACH2* expression was highest in  $T_N$  cells compared with  $T_{CM}$  and  $T_{EM}$  cells. In contrast to  $T_N$  cells, both  $T_{CM}$  and  $T_{EM}$  cells expressed high levels of *IFNG* and *CCR4*. *EOMES* and genes that encode granzymes (*GZMA*, *GZMH*, and *GZMK*) were highly expressed by the  $T_{EM}$  lineage. We identified only a small number of  $T_{CM}$ -specific mRNAs compared with  $T_N$ - and  $T_{EM}$ -specific mRNAs. Next, we input our lineage-specific  $T_N$ ,  $T_{CM}$ , and  $T_{EM}$  gene lists into the Molecular Signature Database (MSigDB, Broad)



(40) and the outputs for these lists were  $T_N$ ,  $T_{CM}$ , and  $T_{EM}$ , respectively. Thus, our isolated cells showed cell type-specific expression of genes encoding lineage-specific cytokines, transcriptional regulators, and effector proteins.

Although the current study was not designed for this purpose, we performed a preliminary analysis to examine lncRNA profiles that may vary due to individual identity. We identified those lncRNAs whose expression varied most according to individual identity and not according to expression in a given  $T_N$ ,  $T_{CM}$ , or  $T_{EM}$  subset. We found that expression of certain lncRNAs seemed to vary more according to individual identity, independent of expression in a specific T cell subset (Fig. 1E). Thus, individual identity also contributes to expression levels of certain lncRNAs in T cell subsets.

We assessed genomic relationships between genes encoding lineage-specific lncRNAs and genes encoding lineage-specific mRNAs as lncRNAs are known to regulate expression of neighboring protein-coding genes and lncRNA - protein-coding gene pairs exhibit cell type-specific coexpression (10). Examples include *IFNG-AS1* and *IFNG* and *TH2LCRR* and *IL4*, *IL5*, and *IL13* (26, 41, 42). We aligned positions of  $T_N$ ,  $T_{CM}$ , and  $T_{EM}$ -specific lncRNA genes with  $T_N$ ,  $T_{CM}$ , and  $T_{EM}$ -specific protein-coding genes across the genome. We used Pearson's linear regression to determine whether lncRNA:mRNA gene pairs were coexpressed in  $T_N$ ,  $T_{CM}$ , and  $T_{EM}$  subsets (see Supplemental Table III for sample calculations). We next analyzed a window of up to 250 kb from the transcription start site of each lncRNA gene to determine genomic distance between coexpressed lncRNA:mRNA gene pairs. For this window, we considered the absolute distance of each lncRNA gene from the nearby coexpressed mRNA gene. We found the highest proportion of lncRNA genes were intragenic with coexpressed mRNA genes (Fig. 2A). We also examined this relationship relative to the number of genes falling within this genomic window and obtained similar results (Fig. 2B). Many lncRNA genes were coexpressed with multiple lineage-specific protein-coding genes in the genome. We found that 51 and 49% of naive- and memory-specific lncRNA genes were transcribed in antisense or sense directions relative to adjacent coexpressed protein-coding genes, respectively (Fig. 2C). Thus, the majority of lineage-specific lncRNA genes were coexpressed with lineage-specific protein-coding genes.

We performed the opposite analysis by determining the frequency that lineage-specific protein-coding genes were near

lineage-specific lncRNA genes in the genome to ask whether lineage-specific protein-coding genes were randomly distributed in the genome or were near lineage-specific lncRNA genes. We found that 58, 27, and 33% of genes encoding  $T_N$ ,  $T_{CM}$ , or  $T_{EM}$ -specific mRNAs were within 300 kb of a gene encoding a  $T_N$ ,  $T_{CM}$ , and  $T_{EM}$ -specific lncRNA, respectively (Fig. 2D). We conclude from these studies that lineage-specific annotated lncRNA and mRNA genes are not randomly distributed across the genome but are colocalized in the genome ( $T_N$ ;  $p = 10^{-22}$ ,  $T_{CM}$ ;  $p = 10^{-12}$ ,  $T_{EM}$ ;  $p = 10^{-14}$ ,  $\chi^2$  analysis).

#### Lineage-specific novel lncRNAs, SEs, and TEs

We expanded our analysis to examine novel or nonannotated lncRNAs expressed in these cell types in a lineage-specific fashion. These transcripts fulfilled criteria of lncRNAs (>200 bp in length and lacked coding potential according to analysis using the coding potential assessment tool, CPAT, and PhyloCSF to estimate evolutionary coding potential). In contrast to the total number of annotated lncRNAs, de novo assembly of our RNA-seq datasets uncovered numerous  $T_N$ ,  $T_{CM}$ , and  $T_{EM}$  lineage-specific lncRNAs as illustrated in the heatmap (Fig. 3A). We also evaluated the extent to which novel lncRNA genes were coexpressed with adjacent protein-coding genes. For comparison, we determined the distances between mRNA genes selectively expressed in the different populations and found a broad distribution between lineage-specific protein-coding genes in the genome (Fig. 3B, left panel). In contrast, when we examined genomic positions of lineage-specific lncRNA loci and coexpressed lineage-specific protein-coding genes, we found that ~50% of lineage-specific lncRNA loci were within 0–50 kb of a lineage-specific mRNA gene and another ~20% were within 50–100 kb of each other (Fig. 3B, right panel). Thus, as with annotated lncRNA loci, lineage-specific novel lncRNA loci exhibited a nonrandom distribution in the genome positioned very near lineage-specific protein-coding genes. We also performed the opposite analysis by determining the frequency at which lineage-specific protein-coding genes were near lineage-specific novel lncRNA genes in the genome to ask whether lineage-specific protein-coding genes were randomly distributed in the genome or were near lineage-specific novel lncRNA genes. We found that 45, 37, and 57% of genes encoding  $T_N$ ,  $T_{CM}$ , or  $T_{EM}$ -specific mRNAs were within 300 kb of a gene encoding a  $T_N$ ,  $T_{CM}$ , or  $T_{EM}$ -specific novel lncRNA, respectively (Fig. 3C). We

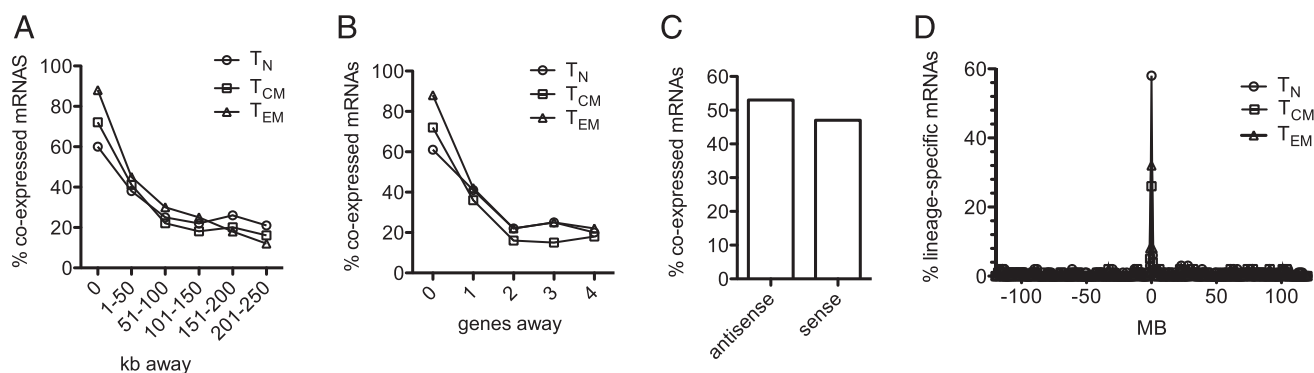
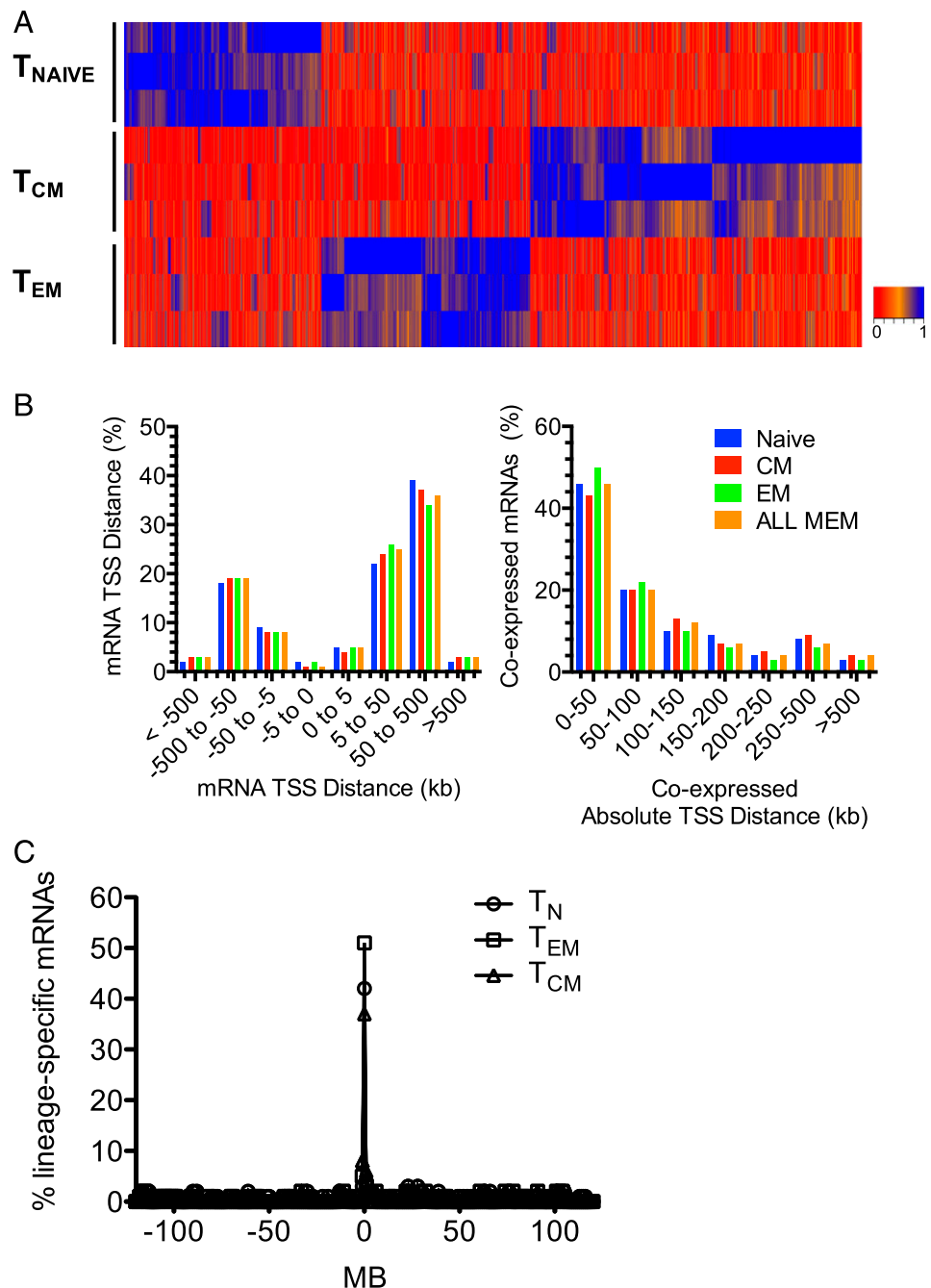


**FIGURE 2.** Relationships between genomic positions of coexpressed lineage-specific protein-coding genes and annotated lncRNA genes. **(A)** Results are expressed as the % of lineage-specific mRNA genes ( $\circ$ ,  $T_N$ ;  $\square$ ,  $T_{CM}$ ;  $\triangle$ ,  $T_{EM}$ ) coexpressed with lineage-specific annotated lncRNA genes relative to total mRNA genes within the indicated distance in kilobase from a lineage-specific annotated lncRNA gene. **(B)** As in (A) except results are expressed relative to the number of genes in the genome away from the lineage-specific annotated lncRNA gene. **(C)** Percentage of coexpressed lineage-specific mRNA genes transcribed in antisense or sense orientations relative to adjacent coexpressed lineage-specific annotated lncRNA genes. **(D)** Genes encoding lineage-specific mRNAs are enriched in the genome near lineage-specific annotated lncRNA genes. The y-axis is the percent of total lineage-specific  $T_N$ ,  $T_{CM}$ , and  $T_{EM}$  mRNAs (Fig. 1, heatmaps). The x-axis is the distance of the gene encoding a lineage-specific mRNA from the nearest gene encoding a lineage-specific annotated lncRNA.  $p$  values determined by  $\chi^2$  analyses,  $T_N$ ,  $p = 10^{-22}$ ,  $T_{CM}$ ,  $p = 10^{-12}$ ,  $T_{EM}$ ,  $p = 10^{-14}$ .

**FIGURE 3.** Discovery of lineage-specific novel lncRNAs. **(A)** Hierarchical clustering showing expression levels of novel lncRNAs expressed by human CD4<sup>+</sup> T<sub>N</sub>, T<sub>CM</sub>, and T<sub>EM</sub> cells determined by whole genome RNA-seq aligned to hg19 ( $n = 3$ ). **(B)** Colocalization of genes encoding lineage-specific mRNAs and novel lncRNAs in the genome. Left panel: % of lineage-specific protein-coding genes that are within the indicated distance in kilobase from another lineage-specific protein-coding gene; right panel: % of lineage-specific protein-coding genes that are within the indicated distance in kilobase from a coexpressed lineage-specific novel lncRNA-coding gene. **(C)** Genes encoding lineage-specific mRNAs are enriched in the genome near lineage-specific novel lncRNA loci. The y-axis is the percent of total lineage-specific T<sub>N</sub>, T<sub>CM</sub>, and T<sub>EM</sub> mRNAs (Fig. 1, heatmaps). The x-axis is the distance of the gene encoding a lineage-specific mRNA from the nearest loci encoding a lineage-specific novel lncRNA.  $p$  values determined by  $\chi^2$  analyses, T<sub>N</sub>,  $p = 10^{-21}$ ; T<sub>CM</sub>,  $p = 10^{-14}$ ; T<sub>EM</sub>,  $p = 10^{-19}$ .



conclude from these studies that lineage-specific novel lncRNA and mRNA genes are not randomly distributed across the genome but are colocalized in the genome ( $p = 10^{-18}$ ,  $10^{-14}$ ,  $10^{-19}$  for T<sub>N</sub>, T<sub>CM</sub>, and T<sub>EM</sub>, respectively,  $\chi^2$  analysis).

#### Relationship between novel lncRNAs and transcriptional enhancers

Transcriptional enhancers are known to express RNAs. We performed genome-wide analyses to further explore the relationship among protein-coding gene loci marked by high levels of lineage-specific novel lncRNAs and lineage-specific transcriptional SEs (43) and TEs identified by levels of H3K27-acetylation marks (20) shown in the Circos plot (Fig. 4A). We employed the following scheme: 1) chromosomes with banding patterns and length in megabases in the outer ring; 2) positions of CD4<sup>+</sup> T<sub>N</sub> and T<sub>M</sub> cell TEs and SEs; and 3) positions of T<sub>N</sub>, T<sub>CM</sub>, and T<sub>EM</sub> lineage-specific novel lncRNAs depicted in that order by the three inner

rings as a function of expression levels. Although somewhat obscure in the Circos plot, we found a large overlap between genomic positions of SEs and TEs present in the different lineages, lineage-specific novel lncRNA loci, and lineage-specific mRNAs. We next ranked lineage-specific mRNAs according to total number of associated lineage-specific novel lncRNAs (Fig. 4B and Supplemental Table IV), SEs according to total number of associated lineage-specific lncRNAs (Fig. 4C) and TEs according to total number of associated lineage-specific lncRNAs (Fig. 4D). Lineage-specific mRNA genes and lineage-specific SEs and TEs had the highest abundance of associated lineage-specific novel lncRNA loci (linear regression analysis,  $R^2 > 0.9$ ,  $p < 0.0001$ ). Genes with a high abundance of lineage-specific lncRNA loci and associated SE and TE density encoded key lineage-specific transcriptional regulators (*BACH2*, *KLF12*, *RORA*, *GATA3*, *ATXN1*, *LEF1*), cytokines (*IFNG*), and receptors (*ICAM2*, *EMR*).

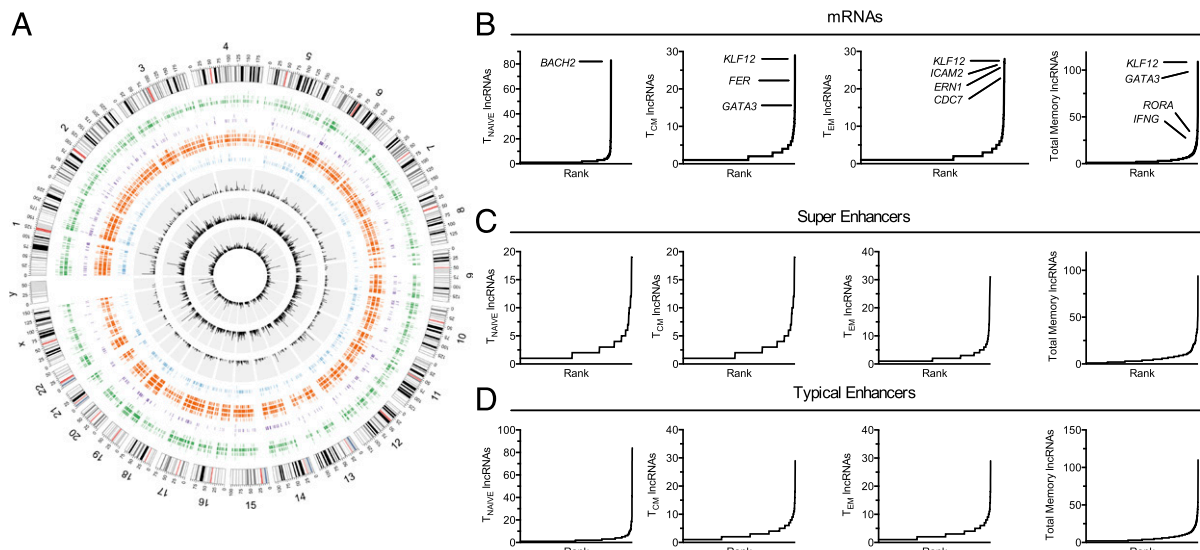


**FIGURE 4.** Relationships among lineage-specific lncRNAs and transcriptional enhancers. **(A)** Circos plot depicting genome-wide positions of CD4-naive typical enhancers and super enhancers (purple) along with CD4 memory typical enhancers (orange) and super enhancers (blue) in the outer rings (from 20). Bar graphs colored in black in the inner concentric circles show lineage-specific novel lncRNAs in naive (outermost), central memory, and effector memory (innermost) cells **(B)** Lineage-specific mRNAs ranked by number of lineage-specific novel lncRNAs per gene loci. Ranks of certain gene loci are noted in the graphs. **(C)** Lineage-specific SE are ranked by number of novel lncRNAs per genomic locus. **(D)** Lineage-specific TEs are ranked by number of novel lncRNAs per genomic locus.

We next determined the distances between expressed novel lncRNA loci in the genome. We found that ~50% of novel lncRNA loci were within 1000 bp of another novel lncRNA loci and >90% were within 10,000 bp of another novel lncRNA genomic loci, suggesting that novel lncRNA loci are clustered in the genome (Fig. 5A). We refer to these small genomic loci that transcribe dense numbers of novel lncRNAs as bins (Fig. 5B). We found that the vast majority of lineage-specific novel lncRNAs were transcribed from these bins that had an average size of <30 kb. Distances between bins were much greater, averaging ~600 kb, indicating the nonrandom distribution of lncRNA loci in the genome. In large part, expression of all the lncRNAs transcribed from an individual bin exhibited lineage-specific expression patterns. Examples include a bin selectively expressed in  $T_N$  (Fig. 5C),  $T_{CM}$  (Fig. 5D), and  $T_{EM}$  (Fig. 5E), respectively.

Given these data, we further analyzed the relationship between genomic positions of  $T_N$  and  $T_M$  cell enhancers and  $T_N$  and  $T_M$  cell bins, and determined the proportion of lineage-specific bins that contained lineage-specific enhancers. We found that lineage-specific bins were highly enriched in the lineage-specific SE and TE portion of the genome (Fig. 5F, 5G). In fact, almost 50% of bins contained at least one lineage-specific SE or TE. Considering that bin loci may not exactly overlap with TE and SE loci, we asked whether expanding bin size in either 5' or 3' directions increased the fraction of bins with TEs or SEs and found that increasing bin size by 20–30 kb increased the proportion of bins with TEs and SEs to ~80%, which was also highly significant. We conclude that positions of lineage-specific bin loci in the genome overlap lineage-specific TE and SE loci.

We reanalyzed the RNA-seq data using bin loci as definition lists, and determined total FPKM expressed from a given bin in  $T_N$ ,  $T_{CM}$ , and  $T_{EM}$  lineages to determine whether bin loci were expressed in selective lineages. After FDR correction, we found that bins could be divided into three categories (Fig. 5H, 5I). About half the bins were highly expressed in  $T_N$  lineages compared with  $T_{CM}$  and  $T_{EM}$  lineages and about half were highly expressed in  $T_{CM}$  and  $T_{EM}$  lineages compared with the  $T_N$  lineage. We identified a small number of bins that were differentially expressed in the  $T_{CM}$  compared with  $T_N$  and  $T_{EM}$  lineages. We conclude that lncRNAs expressed from these bins also exhibit lineage-specific expression.

#### IFNG-associated known and novel lncRNAs

We selected two genes for more detailed investigation: *IFNG* because it is not only selectively expressed by effector Th1 cells and silenced by effector Th2 and Th17 cells but is also expressed by  $T_{EM}$  cells after TCR stimulation, and *BACH2* because it is selectively expressed in  $T_N$  cells and silenced after T cell activation. We found that the *IFNG* gene locus expressed a high density of novel lncRNAs in  $T_{EM}$  and  $T_{CM}$  cells (Fig. 6A). For *IFNG*, we examined RNA-seq tracks (~300 kb) not only in  $T_N$ ,  $T_{CM}$ , and  $T_{EM}$  cells but also in primary and effector Th1, Th2, and Th17 cells (primary, 3 d culture under respective polarizing conditions; effector, 5–7 d culture under the respective polarizing conditions followed by restimulation with anti-CD3 and additional 2 d culture). Similar to  $T_N$  cells, we found a paucity of lncRNAs transcribed by this region in Th2 and Th17 cells (Fig. 6A). In contrast, lncRNAs were highly transcribed from this region by Th1 cells as was *IFNG*, with levels of lncRNAs somewhat higher in effector than primary Th1 cells. lncRNAs transcribed from the *IFNG* locus were similarly elevated in  $T_{CM}$  and  $T_{EM}$  cells, and somewhat higher in  $T_{EM}$  than  $T_{CM}$  cells even though *IFNG* was not actively transcribed by resting  $T_{EM}$  and  $T_{CM}$  cells. Our de novo assembly also identified lncRNAs with defined sizes and genomic locations and these lncRNAs and genomic positions are identified below the RNA-seq tracks. Positions of TEs and SEs based on levels of H3K27-Ac modification in  $T_M$  cells are also shown. We confirmed by RT-PCR that these novel lncRNAs were selectively expressed in  $T_{CM}$  and  $T_{EM}$  cells relative to  $T_N$  cells (Fig. 6B). Each lncRNA transcribed from the *IFNG* locus was named relative to the *IFNG* transcriptional start site in the human genome. For example, for IFNG-R-163, the R is for RNA and -163 means it is transcribed from a position 163 kb from *IFNG* in the direction of the P terminus. RT-PCR was performed using oligo-dT for cDNA synthesis, so our conclusion is that these IFNG-R-lncRNAs are poly-adenylated.

Tes and SEs can be defined by levels of H3K27Ac. JQ1 and I-BET are cell-permeable small molecules that displace BRD-containing proteins from acetylated lysine motifs and disrupt function of TEs and SEs but do not directly reverse H3K27Ac marks

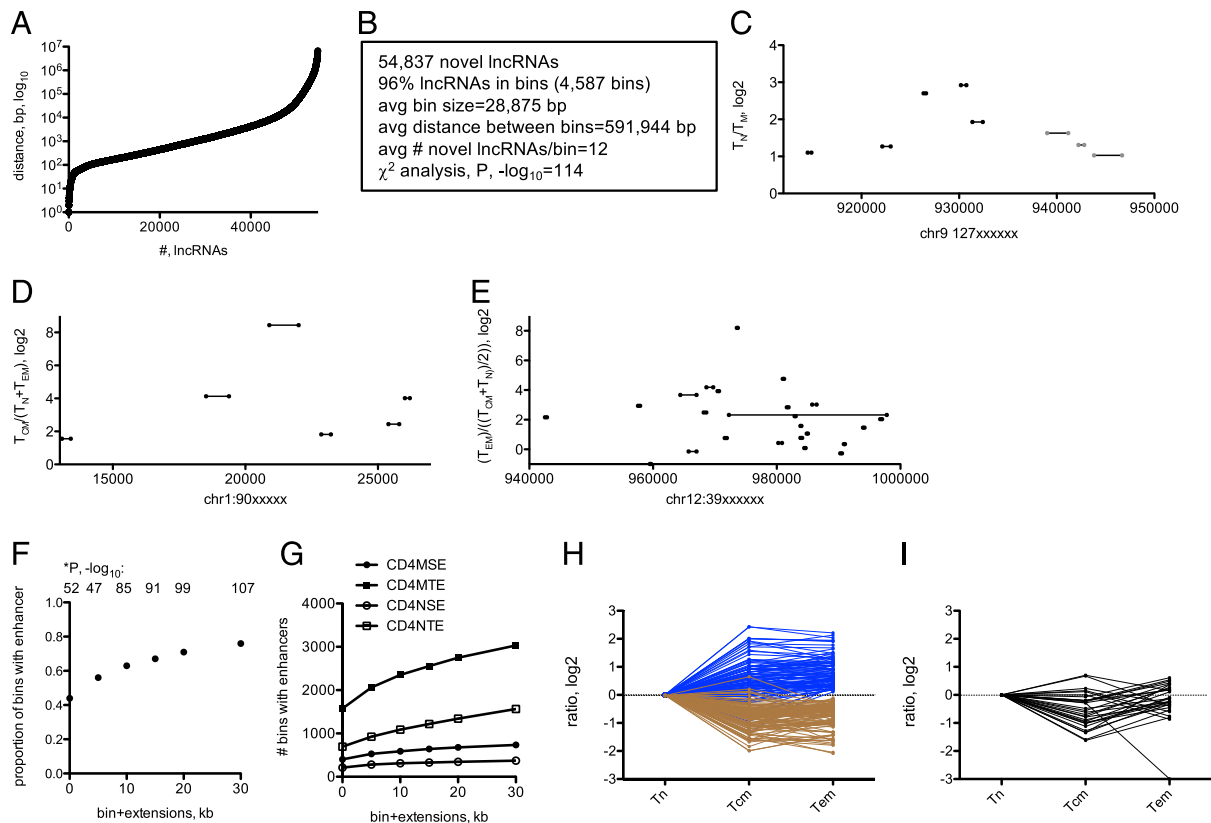


**FIGURE 5.** Genomic distributions of novel lncRNAs. **(A)** Distances between genomic loci transcribing unique novel lncRNAs. The x-axis ranks novel lncRNA loci according to distance to the next novel lncRNA loci and the y-axis shows the actual distance in base pair between neighboring lncRNA loci. **(B)** Characteristics of genomic bins transcribing multiple novel lncRNAs. **(C–E)** Examples of genomic bins selectively transcribing multiple novel lncRNAs in **(C)**  $T_N$  relative to  $T_M$ , **(D)**  $T_{CM}$  relative to  $T_N$  and  $T_{EM}$ , and **(E)**  $T_{EM}$  relative to  $T_N$  and  $T_{CM}$ . The x-axes show genomic positions from which novel lncRNAs are transcribed; lines illustrate sizes of the transcribed novel lncRNA. The y-axes are mean expression ratios, log<sub>2</sub>, between the indicated T cell lineages. **(F)** Genomic bins transcribing novel lncRNAs colocalize with  $T_N$  and  $T_M$  typical and super transcriptional enhancers (from 20). We considered that the genomic bins may not exactly overlap with enhancers so we performed the analysis to include the proportion of bins that colocalize with an enhancer (0), and the proportion of bins that colocalized with enhancers if we extended bin size by 5, 10, 15, 20 or 30 kb in both 5' and 3' directions, x-axis. The y-axis is the proportion of total bins with a  $T_N$  or  $T_M$  enhancer. The  $p$  values,  $-\log_{10}$ , were determined by  $\chi^2$  analysis. **(G)** Number of bins within  $T_M$  SE or TE (CD4MSE, CD4MTE) structures or  $T_N$  SE or TE structures. The x-axis is as in **(F)**, y-axis is the number of bins with enhancers. **(H)** and **(I)** Reanalysis of RNA-seq data using bins as definition lists. **(H)** After FDR correction, bins were identified that were overexpressed (blue lines) or underexpressed (brown lines) in  $T_{CM}$  and  $T_{EM}$  cells compared with  $T_N$  cells. **(I)** Expression levels of bins differentially expressed in  $T_{CM}$  relative to  $T_N$  and  $T_{EM}$  after FDR correction. The y-axes are expression ratios, log<sub>2</sub>; x-axes identify ratios;  $T_N = T_N/T_N$ ,  $T_{CM} = T_{CM}/T_N$ ,  $T_{EM} = T_{EM}/T_N$ .

(35, 44, 45). We also found that the *IFNG* locus spanning ~300 kb (*IFNG*-AS1-*IFNG*-*IL26*) was marked by H3K27Ac in  $T_M$  cells, which was not reversed by treatment with JQ1 (Fig. 6C, left panel). In contrast, RNA pol2 was also recruited to the *IFNG* locus in  $T_M$  cells and RNA pol2 was displaced by treatment with JQ1 (Fig. 6C, right panel). To ask whether lineage-specific novel lncRNA expression at these gene loci was linked to TE or SE function, we studied whether displacement of BRD proteins by JQ1 or I-BET affected levels of novel lncRNAs transcribed from the *IFNG* locus. We found that both JQ1 and I-BET effectively inhibited expression of these lncRNAs in  $T_M$  cells (Fig. 6D). Thus, these novel lncRNA transcripts are consistent with the definition of enhancer-associated RNAs or eRNAs.

Three unique isoforms of the known lncRNA, *IFNG*-AS1, exist in current human genome annotations. Levels of each of these transcripts were also reduced by treatment with JQ1 or I-BET (Fig. 6E). Although *IFNG* is expressed at low levels in resting  $T_M$  cells, it is highly expressed after stimulation via the TCR. We also found that pretreatment with JQ1 or I-BET abrogated induction of *IFNG* expression in  $T_M$  cells (Fig. 6E). Transfection of an siRNA targeting either *IFNG*-AS1 or *IFNG*-R-49 led to marked reduction of both *IFNG* mRNA and protein expression (Fig. 6F). Taken together,

these data demonstrate that both *IFNG*-AS1 and the enhancer-associated RNA, *IFNG*-R-49, are required for efficient induction of *IFNG* by  $T_M$  cells.

#### NF- $\kappa$ B binds novel lncRNAs transcribed from the *IFNG* locus

Recent studies demonstrate that RNAs transcribed from enhancers bind the transcription factor, YY1, as well as the histone acetyltransferase, CBP, to enhance function of these proteins and stimulate transcription of target genes (46, 47). The prosurvival, proinflammatory transcription factor, NF- $\kappa$ B, as well as T-bet, have multiple binding sites across the *IFNG* locus and both are critical for *IFNG* expression (48). Thus, we asked whether one function of the *IFNG*-R lncRNAs was to bind either T-bet or NF- $\kappa$ B. To explore this idea, we performed immunoprecipitations with either anti-T-bet or anti-NF- $\kappa$ B, p65 subunit, and measured *IFNG*-associated lncRNAs in the immunoprecipitates. We failed to detect *IFNG*-associated lncRNAs in the anti-T-bet immunoprecipitates but found that many *IFNG*-associated lncRNAs were detected in the anti-NF- $\kappa$ B immunoprecipitates indicating a portion of these enhancer-associated lncRNAs specifically associate with NF- $\kappa$ B (Fig. 7A, 7B). As a control experiment, we depleted cells of enhancer-associated lncRNAs by JQ1 treatment and found



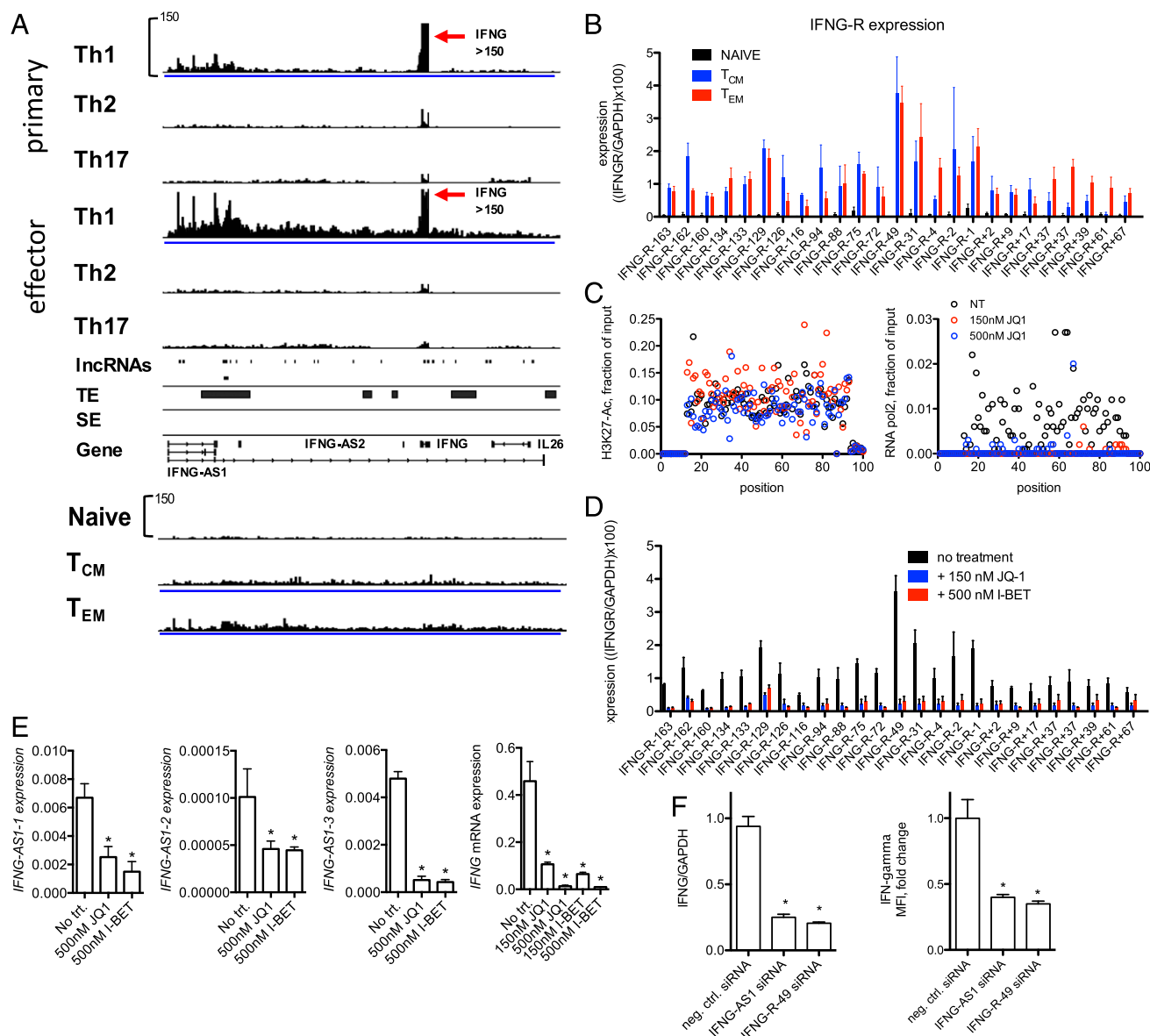


**FIGURE 6.** Novel lncRNAs at the *IFNG* locus. **(A)** RNA-seq tracks spanning ~300 kb from *IFNG*-AS1 past *IL*-26 in primary and effector Th1, Th2 and Th17 cells, naive CD4<sup>+</sup> T cells and T<sub>CM</sub> and T<sub>EM</sub> cells. Below are positions of genomic loci encoding novel lncRNAs determined by de novo assembly, genomic positions of typical and super enhancers (TE and SE, respectively) identified in total CD4<sup>+</sup> T<sub>M</sub> cells are also shown (from Ref. 20). **(B)** PCR validation of RNA-seq results normalized to GAPDH. Each novel lncRNA is named relative to the *IFNG* transcriptional start site, – indicates toward the p-terminus, + toward the q-terminus, differences between either T<sub>CM</sub> and T<sub>N</sub> or T<sub>EM</sub> and T<sub>N</sub> were statistically significant,  $n = 4$ ,  $p < 0.05$ . **(C)** JQ1 treatment of memory T cells abrogates RNA polymerase II binding but not H3K27Ac across the *IFNG* locus. Indicated concentrations of JQ1 were added to T<sub>M</sub> cultures. Cells were stimulated with plate-bound anti-CD3 for 24 h and levels of H3K27-Ac (left panel) and RNA polymerase II (right panel) were determined by ChIP. For this analysis, we designed a tiling array. A total of 100 PCR primer pairs were designed at ~3 kb intervals to span the 300-kb *IFNG* locus. Data are expressed as mean fraction of input ( $n = 3$ )  $p < 0.05$ , ANOVA. **(D)** Total memory CD4<sup>+</sup> T cells were cultured for 24 h with JQ1 or I-BET to displace BRD-containing proteins from genomic loci. RNA was purified and levels of the indicated *IFNG* locus novel lncRNAs, *IFNG*-R-#, determined by PCR. Results are expressed relative to levels of GAPDH.  $p < 0.05$ , treated versus untreated ( $n = 4$ ). **(E)** JQ1 or I-BET inhibit *IFNG*-AS1 and *IFNG* expression. Total memory CD4<sup>+</sup> T cells were treated with and without JQ1 or I-BET for 24 h and stimulated with anti-CD3 for an additional 24 h. Levels of three unique isoforms of *IFNG*-AS1 designated 1, 2, 3 (A), and *IFNG* were determined by PCR and normalized to levels of GAPDH.  $*p < 0.05$  ( $n = 4$ ). **(F)** Individual siRNAs targeting *IFNG*-AS1 or *IFNG*-R-49 were transfected into total memory CD4<sup>+</sup> T cells prior to stimulation with anti-CD3 for 24 h. Transfected cells were isolated by FACS prior to mRNA analysis or to measure intracellular levels of IFN- $\gamma$ . Error bars are mean  $\pm$  SD. The  $p$  values were determined by unpaired  $t$  test.  $*p < 0.05$ .

this treatment also resulted in loss of *IFNG*-associated lncRNAs from the anti-NF- $\kappa$ B immunoprecipitates (Fig. 7B). More importantly, using ChIP assays, we found that treatment of cells with JQ1 resulted in loss of NF- $\kappa$ B binding to chromatin across the *IFNG* locus (Fig. 7C). Next, we reasoned that if *IFNG* enhancer-associated lncRNAs contributed to affinity of NF- $\kappa$ B for *IFNG* locus genomic sites, then treatment of chromatin with RNase may

reduce binding of NF- $\kappa$ B to *IFNG* genomic sites. To explore this possibility, we isolated chromatin without formaldehyde cross-linking, treated chromatin with RNase followed by formaldehyde crosslinking, and processed chromatin for ChIP assays. We found that treatment of chromatin with RNase resulted in loss of NF- $\kappa$ B binding to *IFNG* genomic sites (Fig. 7D). We also treated isolated chromatin from T<sub>M</sub> cells with RNase and found that this treatment

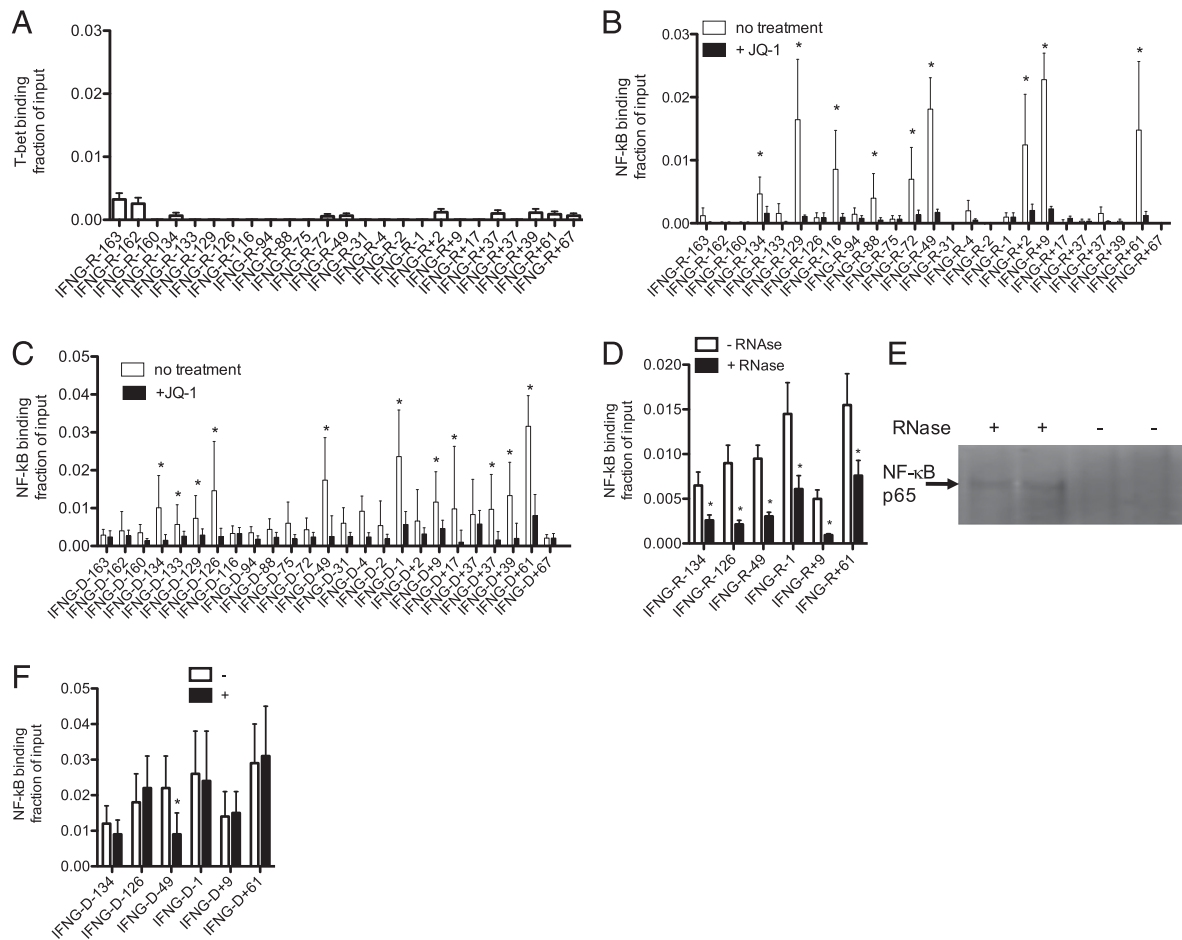


**FIGURE 7.** *IFNG*-associated lncRNAs bind NF- $\kappa$ B. (**A** and **B**) Cells were cultured with or without JQ1 (150 nM, 4 h) and lysed. After lysis, (A) anti-T-bet and (B) anti-NF- $\kappa$ B, p65 subunit, immunoprecipitations (IP) were performed. Levels of each *IFNG*-R-lncRNA in the anti-T-bet, anti-NF- $\kappa$ B, p65 subunit, and isotype control immunoprecipitates were determined by PCR. Results are expressed as fraction of input of the indicated *IFNG*-associated novel lncRNAs relative to totals of each *IFNG*-R-lncRNA. Levels of *IFNG*-R-associated lncRNAs in the isotype control immunoprecipitates were negligible and therefore not included in the calculations. Error bars are SD of eight independent experiments,  $*p < 0.05$ . (**C**) As in (B) except ChIP assays were performed to measure NF- $\kappa$ B, p65, binding to *IFNG* genomic locus sites. Results are expressed as a fraction of input relative to an isotype control. Error bars are SD of five independent experiments,  $*p < 0.05$ . (**D**) Chromatin was isolated from  $T_M$  cells by lysis in nonionic detergents and treated with RNase, 10 min, room temperature. Chromatin was cross-linked with formaldehyde and processed for ChIP assays. NF- $\kappa$ B, p65 binding is expressed as fraction of input,  $n = 3$ ,  $*p < 0.05$  comparing treated and untreated samples. (**E**) After RNase treatment, chromatin was pelleted by centrifugation and supernatant fluids harvested and analyzed for NF- $\kappa$ B protein by Western blotting. The arrow indicates the p65 subunit of NF- $\kappa$ B. (**F**) Cells were transfected with the siRNA targeting *IFNG*-R-49 (+) or a scrambled control siRNA (–) and cultured for 24 h. Cultures were fixed with paraformaldehyde, harvested, and processed for ChIP assays using an NF- $\kappa$ B, p65 subunit, Ab. The y-axis shows NF- $\kappa$ B, p65 subunit, binding as fraction of input at the indicated *IFNG* genomic loci, x-axis.

resulted in release of substantial NF- $\kappa$ B protein from chromatin (Fig. 7E). Finally, we transfected cells with the siRNA specific for *IFNG*-R-49 or a scrambled control siRNA. Transfection of the siRNA specific for *IFNG*-R-49 reduced NF- $\kappa$ B binding to the *IFNG*-D-49 genomic DNA site but not several other sites across the *IFNG* locus (Fig. 7F). Our conclusion is that *IFNG*-enhancer associated lncRNAs contribute to maintaining binding of NF- $\kappa$ B to the *IFNG* locus and in general chromatin-associated RNAs contribute to localization of NF- $\kappa$ B to chromatin, suggesting this notion may have general applicability.

#### Lineage-specific novel lncRNAs at the *BACH2* locus

We used a similar strategy to analyze novel lncRNAs transcribed from the *BACH2* locus in  $T_N$  and  $T_M$  lineages. RNA-seq tracks identified high levels of transcripts across the *BACH2* gene in  $T_N$  cells that were very reduced in  $T_{CM}$  and  $T_{EM}$  cells (Fig. 8A). Our de novo assembly defined >13 unique lncRNAs transcripts preferentially expressed in  $T_N$  compared with  $T_{CM}$  and  $T_{EM}$  cells (Fig. 8B). As above, we confirmed these expression differences by PCR and

obtained similar results (Fig. 8C). We treated  $T_N$  cells with JQ1 and I-BET and found these inhibitors substantially lowered levels of *BACH2*-associated lncRNAs (Fig. 8D) and *BACH2* mRNA (Fig. 8E). Thus, inhibitors that displace BRD proteins from H3K27Ac motifs reduced levels of both *BACH2* enhancer-associated novel lncRNAs and *BACH2* mRNA. Overall, we find these results consistent with the notion that genomic loci surrounding lineage-specific protein-coding genes are enriched with lineage-specific TEs and SEs that transcribe cell type-specific novel lncRNAs.

#### Discussion

The purposes of the investigations presented in this study were to 1) define differential expression patterns of mRNAs, annotated, and novel lncRNAs in human  $T_N$ ,  $T_{CM}$ , and  $T_{EM}$  cells; 2) explore relationships among their expression patterns; and 3) explore relationships among SEs, TEs, and novel lncRNAs. We found that most lineage-specific annotated lncRNAs are coexpressed with adjacent lineage-specific protein-coding genes in the genome, suggesting these annotated lncRNAs contribute to regulation of lineage-specific

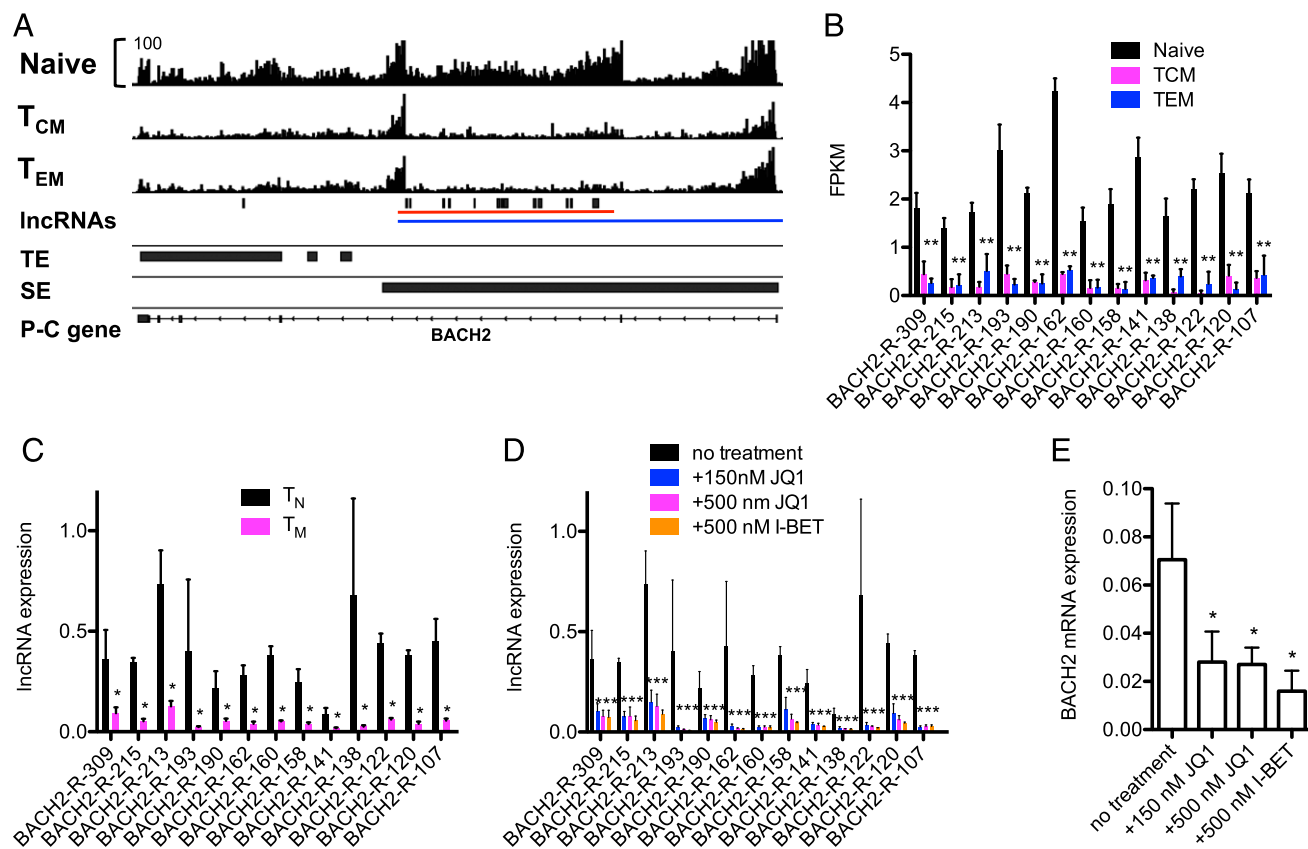


**FIGURE 8.** Novel lncRNAs at the BACH2 locus. **(A)** RNA sequencing tracks of the BACH2 gene in T<sub>N</sub>, T<sub>CM</sub>, and T<sub>EM</sub> cells. Positions of known TEs and SEs in total CD4<sup>+</sup> T cells are shown below the sequencing tracks (from 20). Exon-intron structure of BACH2 is the bottom track. **(B)** Expression levels of the 13 BACH2-associated novel lncRNAs discovered by de novo assembly in T<sub>N</sub>, and T<sub>EM</sub>, and T<sub>CM</sub> expressed as average FPKM,  $n = 3$ ,  $*p < 0.05$ . **(C)** PCR verification of results in (B) expressed relative to GAPDH in T<sub>N</sub> and T<sub>M</sub> cells,  $n = 4$ ,  $*p < 0.05$ . **(D)** T<sub>N</sub> cells were cultured for 24 h with JQ1 or I-BET to displace BRD-containing proteins from genomic loci. RNA was purified and levels of 13 BACH2 associated novel lncRNAs were determined by PCR. Results are expressed relative to levels of GAPDH.  $n = 4$ ,  $*p < 0.05$ . **(E)** As in (D), except levels of BACH2 mRNA were determined by PCR and are expressed relative to GAPDH. The  $p$  values were determined using an unpaired  $t$  test. Error bars are mean  $\pm$  SD,  $*p < 0.05$ .

protein-coding genes and help imprint these very specific cell phenotypes. Previous studies have also defined lineage-specific expression patterns of both annotated and novel lncRNAs in T cells (26, 49, 50). Our de novo assembly identifies many more lineage-specific novel lncRNAs (~15,000) compared with lineage-specific annotated lncRNAs (~200). Expression levels of annotated and novel lncRNAs are comparable and these novel lncRNA loci are also colocalized and coexpressed with lineage-specific protein-coding genes, suggesting they also contribute to regulation of lineage-specific protein-coding genes and underlying cellular phenotypes. Many known lncRNA genes are composed of exons and introns and RNAs are spliced and polyadenylated to yield a mature lncRNA (10). Our de novo assembly reveals that most novel lncRNAs we discovered are polyadenylated but do not undergo splicing to yield mature lncRNAs. This probably explains why we uncovered many more novel lncRNAs compared with annotated lncRNAs described in previous reports (29, 36, 37). These novel lncRNAs are transcribed from enhancer regions found in hematopoietic cells, TEs, and SEs, and inhibition of enhancer function abrogates novel lncRNA expression, suggesting they more closely resemble the class of 1d-eRNAs (17). Lineage-specific expression patterns indicate they are biologically regulated. Transcription of these novel lncRNAs is prevented by inhibition of enhancer function; as is transcription of adjacent lineage-specific protein-coding genes, *IFNG* and *BACH2*, further supporting the notion that their transcription is derived from active enhancers.

Additional roles and mechanisms of regulation of these novel lncRNAs are suggested by our studies. The *IFNG* genomic locus

possesses enhancers specific for *IFNG* and for *IFNG-AS1*, which also regulates *IFNG* expression (48). Both groups of enhancers transcribe novel lncRNAs and are marked by high levels of H3K27Ac and RNA pol2. Both groups of novel lncRNAs are highly regulated during Th cell differentiation in which *IFNG* is actively expressed or actively silenced. However, in resting T<sub>EM</sub> cells, where *IFNG* is not highly expressed, novel lncRNAs are still present at high levels as is the known lncRNA, *IFNG-AS1*. Our results also demonstrate that continued presence of *IFNG*-enhancer-associated novel lncRNAs and *IFNG-AS1* is necessary for rapid expression of *IFNG* by T<sub>EM</sub> cells in response to TCR stimulation. *IFNG-AS1* is known to be required for efficient expression of *IFNG* by murine effector CD4<sup>+</sup> and CD8<sup>+</sup> lymphocytes so it may not seem unexpected that *IFNG-AS1* is also required for efficient expression of *IFNG* by human T<sub>EM</sub> cells (41, 42). However, our results extend the function of *IFNG-AS1* to T<sub>EM</sub> cells. In contrast, it might seem somewhat unexpected that one novel lncRNA, *IFNG-R-49*, transcribed from the *IFNG* locus, is required for efficient expression of *IFNG* by T<sub>EM</sub> cells when numerous novel lncRNAs are transcribed from this locus. However, it is worth noting that multiple transcriptional enhancers have been identified across this locus and several examples exist where deletion of a single 1 kb enhancer is sufficient to abrogate *IFNG* expression by Th1 effector cells and/or T<sub>M</sub> cells (51–53). Novel *IFNG*-associated lncRNAs appear to act, in part, to increase binding of NF- $\kappa$ B to the *IFNG* genomic locus. In separate studies, enhancer-associated lncRNAs have been shown to bind the transcription

factor YY1 and reinforce binding of YY1 to chromatin and bind the histone acetyltransferase, CBP, to stimulate histone acetylation and transcription of target genes (46, 47). Thus, it would appear that one common mechanism by which these novel lncRNAs function at other genomic loci is to reinforce transcription factor and histone acetyltransferase binding to chromatin and function.

One question not completely addressed in this study is the functional relationship between IFNG-AS1 and enhancer-associated RNAs transcribed from the *IFNG* locus. Depletion of either IFNG-AS1 or IFNG-R-49 is sufficient to reduce *IFNG* transcription by T<sub>M</sub> cells. Depletion of IFNG-R-49 also reduces NF-κB binding at IFNG-D-49 but not other enhancer loci. Previous studies suggest that there are distinct NF-κB response enhancers required for IFNG-AS1 expression and distinct NF-κB response enhancers required for *IFNG* expression and both groups of enhancers contribute to expression of *IFNG* by targeting either IFNG-AS1 or *IFNG* genes (48, 54). Two alternate hypotheses that cannot be excluded are 1) that the major role of NF-κB is to drive IFNG-AS1 expression and IFNG-AS1, in turn, drives *IFNG* expression or 2) that the major role of IFNG-AS1 is to drive expression of the IFNG enhancer associated lncRNAs that, in turn reinforce NF-κB binding to *IFNG* enhancer elements and stimulate *IFNG* expression. Additional studies will be required to distinguish among these hypotheses.

Conversely, the transcriptional regulator, *BACH2*, is highly expressed in T<sub>N</sub> cells, represses effector Th programs, and is actively silenced in response to stimulation of Th cell differentiation, and silencing is sustained in T<sub>CM</sub> and T<sub>EM</sub> cells (38). The *BACH2* gene locus transcribes a dense pattern of >80 novel lncRNAs in T<sub>N</sub> cells and these novel lncRNAs are silenced in T<sub>CM</sub> and T<sub>EM</sub> cells. Inhibition of enhancer function in T<sub>N</sub> cells results in the loss of *BACH2*-associated lncRNAs and *BACH2* mRNA, linking these novel lncRNAs to regulation of *BACH2*. Thus, via generation of these novel associated lncRNAs, enhancers may positively regulate expression of protein-coding genes to allow commitment along various cell differentiation paths.

The general argument has been made that genes critically important for cell identity and function, such as *BACH2* and *IFNG*, are marked by SEs and TE and, by extension, these novel enhancer-associated lncRNAs (21). The converse argument, that loci marked by high densities of SEs, TEs, and enhancer-associated lncRNAs may identify genes critical to maintain stability and function of a given cell lineage, such as T<sub>N</sub>, T<sub>CM</sub>, and T<sub>EM</sub> lineages, may also be correct. Therefore, it may be possible to identify new protein-coding genes critical for T<sub>N</sub>, T<sub>CM</sub>, and T<sub>EM</sub> stability and function by ranking them according to SE, TE, and novel lncRNA load as we have done in this study. For example, *KLF12* is marked by high levels of lncRNAs and SEs and TEs in T<sub>M</sub> cells yet the role of this transcription factor in T<sub>M</sub> cell function and stability is poorly understood.

We understand a number of basic mechanisms that annotated lncRNAs employ to achieve their diverse regulatory functions. In contrast, our understanding of biologic functions of enhancer-associated RNAs is more limited (17, 18, 55). One function of RNAs transcribed from TEs and SEs is that they bind the same transcription factors that bind the DNA elements from which the RNA is transcribed, and these eRNAs help tether transcription factors to these regulatory DNA elements, which in turn stabilizes gene-expression programs and reinforces cell phenotypes (46). Our studies are consistent with this type of mechanism. Other studies suggest that eRNAs may contribute to chromosome conformation and nuclear localization (56). Additional studies will be required to fully understand the diverse functions of this class of RNAs, not only in immunological memory, but also how they contribute to biologic complexity in general. Nevertheless, our

results support the notion that both annotated lncRNAs and enhancer-associated lncRNAs play critical roles in maintaining the identity of these key T cell lineages, enabling these cells to carry out their unique adaptive immune functions.

A major difference between T<sub>N</sub> and T<sub>M</sub> cells is that T<sub>N</sub> cells require TCR signaling and additional stimuli, such as cytokine receptor stimulation, to induce or activate a number of transcription factors that initiate differentiation paths, making these cells competent to produce key inflammatory cytokines, chemokines, and other proteins required by the adaptive immune response, whereas T<sub>M</sub> cells only require TCR signaling. This is also revealed by the transcription factor requirements to induce these genes. For example, Stat4, T-bet, NF-κB, and other transcription factors play key roles in the induction of *IFNG* by developing Th1 cells whereas rapid *IFNG* expression by T<sub>M</sub> cells is relatively Stat4 and T-bet independent but still NF-κB dependent, and TCR signaling alone is sufficient to activate NF-κB (6, 57). We propose that expression of enhancer-associated lncRNAs enables NF-κB recruitment to the *IFNG* locus by T-bet/Stat4-independent mechanisms driving rapid expression of *IFNG* by T<sub>M</sub> cells, thus reducing transcription factor requirements for expression of this key gene of the memory response. This underlying mechanism may also contribute to sustained and inducible expression of other key protein-coding genes, allowing T<sub>M</sub> cells to carry out their unique functions providing lifelong immunity against pathogens, a key element of the adaptive immune response.

## Disclosures

The authors have no financial conflicts of interest.

## References

- MacLeod, M. K. L., E. T. Clambey, J. W. Kappler, and P. Marrack. 2009. CD4 memory T cells: what are they and what can they do? *Semin. Immunol.* 21: 53–61.
- Marshall, H. D., A. Chandele, Y. W. Jung, H. Meng, A. C. Poholek, I. A. Parish, R. Rutishauser, W. Cui, S. H. Kleinstein, J. Craft, and S. M. Kaech. 2011. Differential expression of Ly6C and T-bet distinguish effector and memory Th1 CD4(+) cell properties during viral infection. *Immunity* 35: 633–646.
- Pepper, M., and M. K. Jenkins. 2011. Origins of CD4(+) effector and central memory T cells. *Nat. Immunol.* 12: 467–471.
- Sallusto, F., J. Geginat, and A. Lanzavecchia. 2004. Central memory and effector memory T cell subsets: function, generation, and maintenance. *Annu. Rev. Immunol.* 22: 745–763.
- Sallusto, F., D. Lenig, R. Förster, M. Lipp, and A. Lanzavecchia. 1999. Two subsets of memory T lymphocytes with distinct homing potentials and effector functions. *Nature* 401: 708–712.
- Zhu, J., H. Yamane, and W. E. Paul. 2010. Differentiation of effector CD4 T cell populations (\*). *Annu. Rev. Immunol.* 28: 445–489.
- Chang, J. T., E. J. Wherry, and A. W. Goldrath. 2014. Molecular regulation of effector and memory T cell differentiation. *Nat. Immunol.* 15: 1104–1115.
- Hangauer, M. J., I. W. Vaughn, and M. T. McManus. 2013. Pervasive transcription of the human genome produces thousands of previously unidentified long intergenic noncoding RNAs. *PLoS Genet.* 9: e1003569.
- Chang, H. Y. 2013. Genome regulation by long noncoding RNAs. *Cancer Res.* 73: SY31-03 (Abstr.).
- Rinn, J. L., and H. Y. Chang. 2012. Genome regulation by long noncoding RNAs. *Annu. Rev. Biochem.* 81: 145–166.
- Zambelli, F., and G. Pavesi. 2015. RIP-Seq data analysis to determine RNA-protein associations. *Methods Mol. Biol.* 1269: 293–303.
- Liu, G., J. S. Mattick, and R. J. Taft. 2013. A meta-analysis of the genomic and transcriptional composition of complex life. *Cell Cycle* 12: 2061–2072.
- Mousavi, K., H. Zare, S. Dell'orso, L. Grontved, G. Gutierrez-Cruz, A. Derfoul, G. L. Hager, and V. Sartorelli. 2013. eRNAs promote transcription by establishing chromatin accessibility at defined genomic loci. *Mol. Cell* 51: 606–617.
- Lam, M. T. Y., W. Li, M. G. Rosenfeld, and C. K. Glass. 2014. Enhancer RNAs and regulated transcriptional programs. *Trends Biochem. Sci.* 39: 170–182.
- Ren, B. 2010. Transcription: enhancers make non-coding RNA. *Nature* 465: 173–174.
- Koch, F., R. Fenouil, M. Gut, P. Cauchy, T. K. Albert, J. Zacarias-Cabeza, S. Spicuglia, A. L. de la Chapelle, M. Heidemann, C. Hintermair, et al. 2011. Transcription initiation platforms and GTF recruitment at tissue-specific enhancers and promoters. *Nat. Struct. Mol. Biol.* 18: 956–963.
- Natoli, G., and J. C. Andrau. 2012. Noncoding transcription at enhancers: general principles and functional models. *Annu. Rev. Genet.* 46: 1–19.
- Li, W., D. Notani, and M. G. Rosenfeld. 2016. Enhancers as non-coding RNA transcription units: recent insights and future perspectives. *Nat. Rev. Genet.* 17: 207–223.



19. Jacquier, A. 2009. The complex eukaryotic transcriptome: unexpected pervasive transcription and novel small RNAs. *Nat. Rev. Genet.* 10: 833–844.
20. Hnisz, D., B. J. Abraham, T. I. Lee, A. Lau, V. Saint-André, A. A. Sigova, H. A. Hoke, and R. A. Young. 2013. Super-enhancers in the control of cell identity and disease. *Cell* 155: 934–947.
21. Whyte, W. A., D. A. Orlando, D. Hnisz, B. J. Abraham, C. Y. Lin, M. H. Kagey, P. B. Rahl, T. I. Lee, and R. A. Young. 2013. Master transcription factors and mediator establish super-enhancers at key cell identity genes. *Cell* 153: 307–319.
22. Vahedi, G., Y. Kanno, Y. Furumoto, K. Jiang, S. C. Parker, M. R. Erdos, S. R. Davis, R. Roychoudhuri, N. P. Restifo, M. Gadina, et al. 2015. Super-enhancers delineate disease-associated regulatory nodes in T cells. *Nature* 520: 558–562.
23. Peeters, J. G., S. J. Vervoort, S. C. Tan, G. Mijneer, S. de Rooij, S. J. Vastert, E. E. Nieuwenhuis, F. van Wijk, B. J. Prakken, M. P. Creighton, et al. 2015. Inhibition of super-enhancer activity in autoimmune disease-derived T cells reduces disease-associated gene expression. *Cell Rep.* 12: 1986–1996.
24. Chapuy, B., M. R. McKeown, C. Y. Lin, S. Monti, M. G. Roemer, J. Qi, P. B. Rahl, H. H. Sun, K. T. Yeda, J. G. Doench, et al. 2013. Discovery and characterization of super-enhancer-associated dependencies in diffuse large B cell lymphoma. [Published erratum appears in 2014 *Cancer Cell* 25: 545–546.] *Cancer Cell* 24: 777–790.
25. Chang, S., and T. M. Aune. 2007. Dynamic changes in histone-methylation ‘marks’ across the locus encoding interferon-gamma during the differentiation of T helper type 2 cells. *Nat. Immunol.* 8: 723–731.
26. Spurlock III, C. F., J. T. Tossberg, Y. Guo, S. P. Collier, P. S. Crooke, III, and T. M. Aune. 2015. Expression and functions of long noncoding RNAs during human T helper cell differentiation. *Nat. Commun.* 6: 6932.
27. Spurlock III, C. F., J. T. Tossberg, B. K. Matlock, N. J. Olsen, and T. M. Aune. 2014. Methotrexate inhibits NF- $\kappa$ B activity via long intergenic (noncoding) RNA-p21 induction. *Arthritis Rheumatol.* 66: 2947–2957.
28. Guo, Y., F. Ye, Q. Sheng, T. Clark, and D. C. Samuels. 2014. Three-stage quality control strategies for DNA re-sequencing data. *Brief. Bioinform.* 15: 879–889.
29. Guo, Y., S. Zhao, Q. Sheng, F. Ye, J. Li, B. Lehmann, J. Pieterpol, D. C. Samuels, and Y. Shyr. 2014. Multi-perspective quality control of Illumina exome sequencing data using QC3. *Genomics* 103: 323–328.
30. Guo, Y., S. Zhao, F. Ye, Q. Sheng, and Y. Shyr. 2014. MultiRankSeq: multi-perspective approach for RNAseq differential expression analysis and quality control. *BioMed Res. Int.* 2014: 248090.
31. Kim, D., G. Pertea, C. Trapnell, H. Pimentel, R. Kelley, and S. L. Salzberg. 2013. TopHat2: accurate alignment of transcriptomes in the presence of insertions, deletions and gene fusions. *Genome Biol.* 14: R36.
32. Trapnell, C., A. Roberts, L. Goff, G. Pertea, D. Kim, D. R. Kelley, H. Pimentel, S. L. Salzberg, J. L. Rinn, and L. Pachter. 2012. Differential gene and transcript expression analysis of RNA-seq experiments with TopHat and Cufflinks. *Nat. Protoc.* 7: 562–578.
33. Trapnell, C., B. A. Williams, G. Pertea, A. Mortazavi, G. Kwan, M. J. van Baren, S. L. Salzberg, B. J. Wold, and L. Pachter. 2010. Transcript assembly and quantification by RNA-Seq reveals unannotated transcripts and isoform switching during cell differentiation. *Nat. Biotechnol.* 28: 511–515.
34. Cervera, R., M. A. Khamashta, J. Font, G. D. Sebastiani, A. Gil, P. Lavilla, J. C. Mejía, A. O. Aydin, H. Chwalinska-Sadowska, E. de Ramón, et al. European Working Party on Systemic Lupus Erythematosus. 2003. Morbidity and mortality in systemic lupus erythematosus during a 10-year period: a comparison of early and late manifestations in a cohort of 1,000 patients. *Medicine (Baltimore)* 82: 299–308.
35. Nagarajan, S., T. Hossan, M. Alawi, Z. Najafova, D. Indenbirken, U. Bedi, H. Taipaleenmäki, I. Ben-Batalla, M. Scheller, S. Loges, et al. 2014. Bromodomain protein BRD4 is required for estrogen receptor-dependent enhancer activation and gene transcription. *Cell Rep.* 8: 460–469.
36. Alvarez-Dominguez, J. R., W. Hu, B. Yuan, J. Shi, S. S. Park, A. A. Gromatzky, A. van Oudenaarden, and H. F. Lodish. 2014. Global discovery of erythroid long noncoding RNAs reveals novel regulators of red cell maturation. *Blood* 123: 570–581.
37. Tsukumo, S., M. Unno, A. Muto, A. Takeuchi, K. Kometani, T. Kurosaki, K. Igarashi, and T. Saito. 2013. Bach2 maintains T cells in a naive state by suppressing effector memory-related genes. *Proc. Natl. Acad. Sci. USA* 110: 10735–10740.
38. Roychoudhuri, R., K. Hirahara, K. Mousavi, D. Clever, C. A. Klebanoff, M. Bonelli, G. Sciumè, H. Zare, G. Vahedi, B. Dema, et al. 2013. BACH2 represses effector programs to stabilize T(reg)-mediated immune homeostasis. *Nature* 498: 506–510.
39. Kuwahara, M., J. Suzuki, S. Tofukuji, T. Yamada, M. Kanoh, A. Matsumoto, S. Maruyama, K. Kometani, T. Kurosaki, O. Ohara, et al. 2014. The Menin-Bach2 axis is critical for regulating CD4 T-cell senescence and cytokine homeostasis. *Nat. Commun.* 5: 3555.
40. Subramanian, A., P. Tamayo, V. K. Mootha, S. Mukherjee, B. L. Ebert, M. A. Gillette, A. Paulovich, S. L. Pomeroy, T. R. Golub, E. S. Lander, and J. P. Mesirov. 2005. Gene set enrichment analysis: a knowledge-based approach for interpreting genome-wide expression profiles. *Proc. Natl. Acad. Sci. USA* 102: 15545–15550.
41. Collier, S. P., P. L. Collins, C. L. Williams, M. R. Boothby, and T. M. Aune. 2012. Cutting edge: influence of Tmevp1, a long intergenic noncoding RNA, on the expression of Ifng by Th1 cells. *J. Immunol.* 189: 2084–2088.
42. Gomez, J. A., O. L. Wapinski, Y. W. Yang, J. F. Bureau, S. Gopinath, D. M. Monack, H. Y. Chang, M. Brahic, and K. Kirkegaard. 2013. The NeST long ncRNA controls microbial susceptibility and epigenetic activation of the interferon- $\gamma$  locus. *Cell* 152: 743–754.
43. Koh, J. L., Y. T. Chong, H. Friesen, A. Moses, C. Boone, B. J. Andrews, and J. Moffat. 2015. CYCLOPs: a comprehensive database constructed from automated analysis of protein abundance and subcellular localization patterns in *Saccharomyces cerevisiae*. *G3 (Bethesda)* 5: 1223–1232.
44. Delmore, J. E., G. C. Issa, M. E. Lemieux, P. B. Rahl, J. Shi, H. M. Jacobs, E. Kastiris, T. Gilpatrick, R. M. Paranal, J. Qi, et al. 2011. BET bromodomain inhibition as a therapeutic strategy to target c-Myc. *Cell* 146: 904–917.
45. Nicodem, E., K. L. Jeffrey, U. Schaefer, S. Beinke, S. Dewell, C. W. Chung, R. Chandwani, I. Marazzi, P. Wilson, H. Coste, et al. 2010. Suppression of inflammation by a synthetic histone mimic. *Nature* 468: 1119–1123.
46. Sigova, A. A., B. J. Abraham, X. Ji, B. Molin, N. M. Hannett, Y. E. Guo, M. Jang, C. C. Giallourakis, P. A. Sharp, and R. A. Young. 2015. Transcription factor trapping by RNA in gene regulatory elements. *Science* 350: 978–981.
47. Bose, D. A., G. Donahue, D. Reinberg, R. Shiekhattar, R. Bonasio, and S. L. Berger. 2017. RNA binding to CBP stimulates histone acetylation and transcription. *Cell* 168: 135–149 e122.
48. Collier, S. P., M. A. Henderson, J. T. Tossberg, and T. M. Aune. 2014. Regulation of the Th1 genomic locus from Ifng through Tmevp1 by T-bet. *J. Immunol.* 193: 3959–3965.
49. Ranzani, V., G. Rossetti, I. Panzeri, A. Arrigoni, R. J. Bonnal, S. Curti, P. Gruarin, E. Provasi, E. Sugliano, M. Marconi, et al. 2015. The long intergenic noncoding RNA landscape of human lymphocytes highlights the regulation of T cell differentiation by linc-MAF-4. *Nat. Immunol.* 16: 318–325.
50. Hu, G., Q. Tang, S. Sharma, F. Yu, T. M. Escobar, S. A. Muljo, J. Zhu, and K. Zhao. 2013. Expression and regulation of intergenic long noncoding RNAs during T cell development and differentiation. *Nat. Immunol.* 14: 1190–1198.
51. Collins, P. L., S. Chang, M. Henderson, M. Soutto, G. M. Davis, A. G. McLeod, M. J. Townsend, L. H. Glimcher, D. P. Mortlock, and T. M. Aune. 2010. Distal regions of the human IFNG locus direct cell type-specific expression. *J. Immunol.* 185: 1492–1501.
52. Collins, P. L., M. A. Henderson, and T. M. Aune. 2012. Lineage-specific adjacent IFNG and IL26 genes share a common distal enhancer element. *Genes Immun.* 13: 481–488.
53. Collins, P. L., M. A. Henderson, and T. M. Aune. 2012. Diverse functions of distal regulatory elements at the IFNG locus. *J. Immunol.* 188: 1726–1733.
54. Balasubramani, A., Y. Shibata, G. E. Crawford, A. S. Baldwin, R. D. Hatton, and C. T. Weaver. 2010. Modular utilization of distal cis-regulatory elements controls Ifng gene expression in T cells activated by distinct stimuli. *Immunity* 33: 35–47.
55. St Laurent, G., C. Wahlestedt, and P. Kapranov. 2015. The Landscape of long noncoding RNA classification. *Trends Genet.* 31: 239–251.
56. Li, W., D. Notani, Q. Ma, B. Tanasa, E. Nunez, A. Y. Chen, D. Merkurjev, J. Zhang, K. Ohgi, X. Song, et al. 2013. Functional roles of enhancer RNAs for oestrogen-dependent transcriptional activation. *Nature* 498: 516–520.
57. Lai, W., M. Yu, M. N. Huang, F. Okoye, A. D. Keegan, and D. L. Farber. 2011. Transcriptional control of rapid recall by memory CD4 T cells. *J. Immunol.* 187: 133–140.